Amplitude stabilization and active control of a terahertz quantum cascade laser with a graphene loaded split-ring-resonator array

B. Wei[1,*], S. J. Kindness[1], N. W. Almond[1], R. Wallis[1], Y. Wu[1], Y. Ren[2,3], S. C. Shi[2,3], P. Braeuninger-Weimer[4], S. Hofmann[4], H. E. Beere[1], D. A. Ritchie[1], and R. Degl'lnnocenti[5]

[1]*Cavendish Laboratory, University of Cambridge, J J Thomson Avenue, Cambridge, CB3 0HE, United Kingdom*
[2]*Purple Mountain Observatory, Chinese Academy of Sciences, 8 Yuanhua Road, Nanjing, Jiangsu, 210034, China*
[3]*Key Laboratory of Radio Astronomy, Chinese Academy of Sciences, 8 Yuanhua Road, Nanjing, Jiangsu, 210034, China*
[4]*Dept. of Engineering, University of Cambridge, 9 J J Thomson Avenue, Cambridge, CB3 0FA, United Kingdom*
[5]*Dept. of Engineering, Lancaster University, Engineering building, Lancaster, LA1 4YW, United Kingdom*

**bw373@cam.ac.uk*

Abstract: We demonstrate the amplitude stabilization of a 2.85 THz quantum cascade laser with a graphene loaded split-ring-resonator array, acting as an external amplitude modulator. The transmittance of the modulator can be actively changed by modifying the graphene conductivity via electrostatic back-gating. The modulator operates at room temperature and is capable of actively modulating the quantum cascade laser power level and thus stabilizing the power output via a proportional-integral-derivative feedback control loop. The stability was enhanced by more than 10 times through actively tuning the modulation. Furthermore, this approach can be used to externally control the laser power with a high level of stability.

Terahertz (THz) quantum cascade lasers are widely used solid-state sources for astronomical applications[1], imaging[2], and spectroscopy[3] because of their high output power[4] and narrow spectral linewidth[5]. During astronomical observations, long integration times are required to achieve a suitable signal to noise (S/N) ratio, which requires the amplitude of the light source to be kept stable within the integration time[6]. However, the output power of a quantum cascade laser (QCL) is sensitive to temperature fluctuations[7], which are intrinsically present in the cryostat used to cool the laser[8]. In addition, light propagating through an external unpurged atmosphere suffers from extra power fluctuations due to the strong THz absorption[9]. Therefore, it is of great importance to realize an active stabilization of the output laser power. For imaging, it is also important to have a stabilized THz source for conducting accurate quantitative measurements of a sample. In QCL-assisted spectroscopic applications[10], active amplitude stabilization is also required, e.g., when monitoring the presence/concentration of noxious or greenhouse gases with high precision. At the same time, THz wireless communication is a promising application of THz sources, and there have already been demonstrations of high bit rate sub-THz communications[11,12]. In many protocols for communication applications, precise control of the laser intensity is required, thus aiding the reduction in bit error rate.

To achieve amplitude stabilization, an active amplitude modulator is typically required, and graphene loaded metamaterial arrays provide an extremely promising solution, particularly in terms of modulation depth and speed[13] and ease of implementation[14]. Metamaterials provide strong confinement of electromagnetic radiation at a designed frequency[15], primarily determined by the shape and size of the resonant unit, rather than its material composition, and are normally engineered as metallic features on a dielectric substrate. The electrical conductivity of graphene can be significantly tuned by modifying the carrier concentration[16]. The combination of these concepts is the key to achieving efficient tunable reflectivity within a certain frequency range. To date, many THz modulators have been developed based on graphene loaded metamaterials[17]. Graphene loaded split ring resonators (SRR) operating with ultra-low bias have been demonstrated[18,19], and 100% modulation depths have been achieved by combining an active metamaterial with a THz QCL[20].

In this work, we demonstrate amplitude stabilization and active intensity control of a THz QCL using an external active amplitude modulator utilizing hybrid metamaterial/graphene SRR arrays. The experimental

apparatus has been designed to operate in transmission with the hybrid graphene-SRR modulator placed externally to the cryostat. An illustration of the setup is shown in Fig. 1 (a). A proportional-integral-derivative (PID) loop controller was used to actively adjust the gate voltage of the SRR to compensate for the power fluctuation of the laser.

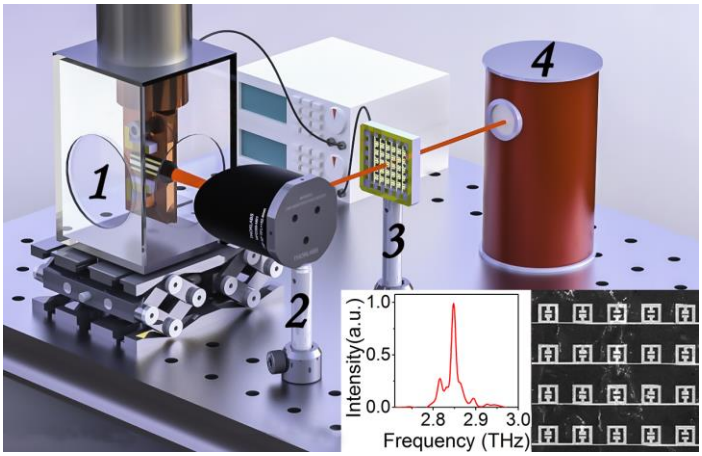

(a)

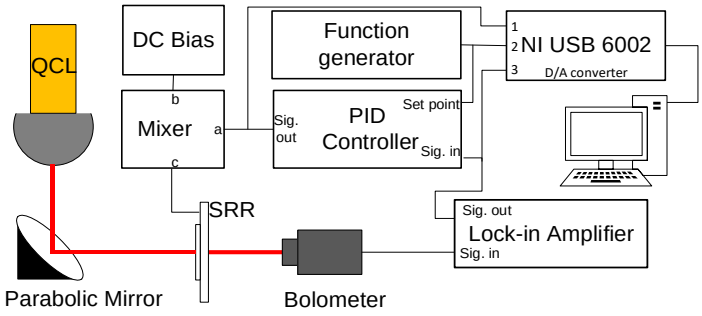

(b)

FIG. 1. (a) Illustration and (b) schematic of the set-up for amplitude stabilization: 1) cryostat and QCL; 2) off-axis parabolic mirror; 3) SRR; 4) bolometer. The spectrum of the QCL and a SEM micrograph of the SRR device is shown at the bottom right corner of a).

Fig. 1 (b) shows a schematic of the electronic components implemented for the amplitude stabilization and control of the QCL. The light source is a 2.85 THz single-plasmon QCL with a bound-to-continuum active region design[21]. The spectrum of the laser output at maximum power is shown in the inset of Fig. 1 (a), with a main emission peak at 2.85 THz. The QCL is mounted onto a cold finger in a continuous flow He cryostat, the temperature of which was held at 5K with an average observed fluctuation of +/-0.2K. The laser is operated in pulsed mode with a repetition rate of 10 kHz and a 5% duty cycle. CW emission is compatible with this approach by simply modifying the experimental setup with an additional beam-splitter and an optical chopper. A 4 mm diameter uncoated high-resistivity hyper-hemispherical Si lens was attached on the facet of the laser to collimate the beam and an off-axis parabolic mirror was then used to focus the collimated beam onto the hybrid graphene-SRR array, which is 3×3 mm^2. This experiment was conceived as a proof-of-principle, and therefore a large area SRR array was used for ease of alignment.

The output power of the laser after passing through the SRR device was collected with a liquid-He cooled Si-bolometer chosen for its high S/N ratio and relatively high frequency response (up to 2 kHz), which are important features for an accurate PID control. In principle it could be possible to use similar integrated devices[22,23] as both detectors and modulators, removing the need for an external cryogenic detector and extending the PID control bandwidth. However, in this first demonstration of amplitude stabilization a more

conventional, higher responsivity cryogenic Si bolometer detector was used to allow an optimal experimental set-up. The signal recorded by the bolometer is first extracted by a lock-in amplifier at a reference frequency of 1 kHz, which is also the gate frequency given to the QCL, and then sent to the PID controller. This generates a DC output when the signal from the bolometer deviates from a designated setpoint, which can be adjusted to determine the target power of the laser after transmission through the SRR device. The output voltage range of the PID controller was -10 V to 10 V. This DC output is applied on the back gate of the SRR device to control its transmission properties, thus compensating any change in laser power.

Three signals were finally recorded, the output power of the laser, the setpoint of the PID controller and the output voltage of the PID controller. To achieve high speed data transmission, the signals were acquired using a NI USB 6002 DAQ device with a maximum sample rate of 50,000 samples per second and 8 analogue input channels, before recording on a computer through a LabVIEW program.

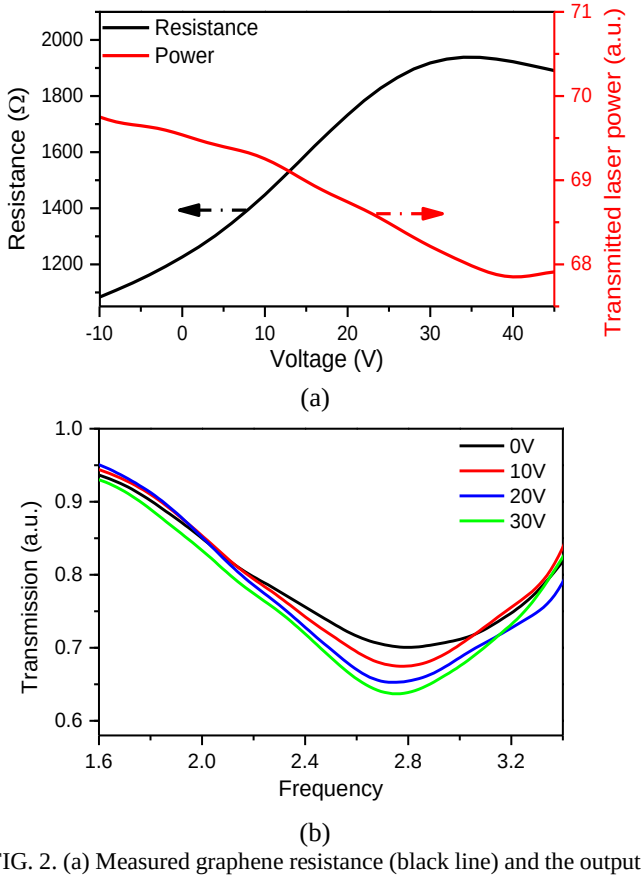

FIG. 2. (a) Measured graphene resistance (black line) and the output power of an external cavity laser (red line) for different back-gate voltage; (b) Transmission spectra of the SRR at four different voltages measured with a THz-TDS system.

The SRR-graphene device was fabricated with the same procedure as the one reported in reference [20]. It was designed to have a resonant frequency at 2.85 THz, overlapping with the frequency of the QCL. The size of a unit cell is 22.5 × 22.5 μm^2 for a total area of 3 × 3 mm^2. CVD graphene is used[24] for the device and the graphene is encapsulated by a 100 nm layer of Al_2O_3 deposited via atomic layer deposition (ALD). The stop-flow mode ALD technique is used to uniformly deposit an encapsulation layer on the graphene which is continuous and pin-hole free, resulting in a higher graphene mobility. This layer also passivates the graphene, inhibiting any Dirac point drift to higher voltages when exposed to the ambient environment.

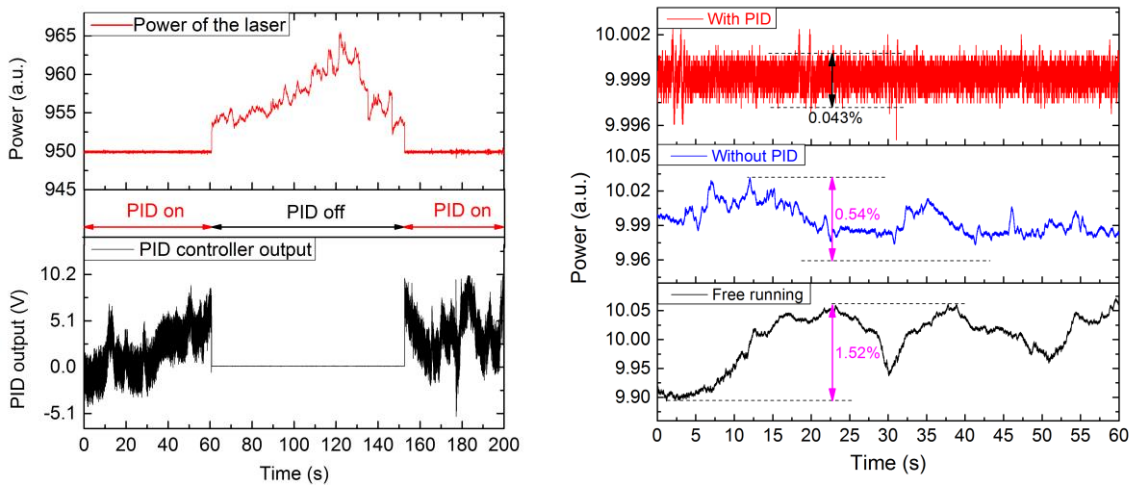

(a) (b)

FIG. 3. (a) The power fluctuation of the laser (red line) with the PID on (0 s to 60 s, 153 s to 200 s) and off (60 s to 153 s) and the corresponding output of the PID controller (black line); (b) The output power fluctuation within 60 seconds of a laser with a PID controlled SRR modulator (red line), the same laser with the SRR modulator but no PID control (blue line), and a free running laser (black line). The power of the free running laser has been normalized to the same level as the other two traces for comparison.

The graphene sheet conductivity was extracted by measuring the resistance across the area at different back-gate voltages. The location of maximum resistance was identified as the Dirac point, around 35 V, as shown in the black line in Fig. 2 (a), compatible with p-doped CVD grown graphene. An optical characterization of the SRR device was performed with the setup shown in Fig. 1 (b). The output power of the laser after transmitting through the SRR was recorded with different back-gate voltages. The red line in Fig. 2 (a) shows the result, which is consistent with the resistance measurements. The SRR reflectivity is maximal at the graphene Dirac point, and therefore when the device is biased at such a voltage the transmission power from the laser is at a minimum. As can be seen from the red line in Fig. 2 (a), the Dirac point of the device drifts by 4 V (from 35 V to 39 V), which is suspected to be due to the hysteresis of the graphene charges, as observed for this type of device[25], and in agreement with our previous measurements. The device was also characterized with a THz time-domain spectroscopic (THz-TDS) system (Menlosystems, model K-15) in the transmission configuration, which was chosen to match the configuration adopted for amplitude stabilization measurements. Fig. 2 (b) gives the transmission spectra of the device at 0V, 10, 20V and 30V. According to the spectra, the device has a resonance at approximately 2.85 THz, and the transmittivity increases by 3% when the back-gate voltage is changed from 10 V to 30 V, in good agreement with the reflectivity and resistance measurements presented in Fig. 2 (a).

As can be seen from Fig. 2 (a), if the back-gate voltage of the SRR is changed from -10 V to 10 V, a limited power modulation is achievable, because of the reduced corresponding conductivity change. However, when a 20 V offset is given onto the back-gate voltage, an output power modulation of 1.6% was recorded, which is sufficient to provide robust amplitude stabilization. Additionally, to keep the PID control loop stable and not induce oscillation into the system, the transmittivity should change monotonically with increasing back-gate voltage. Considering these two arguments, a 20 V DC offset was added onto the output of the PID controller through a DC mixer, and the mixed voltage was applied to the back-gate of the SRR array. When the laser power through the SRR modulator increases, as measured by the bolometer, the feedback loop generates a positive output which lowers the transmission through the SRR, and vice versa. Therefore, the power transmitted through the SRR can be kept stable with a properly applied PID parameter set.

Two sets of experiments were conducted with this system: amplitude stabilization and active control of the amplitude. In the first experiment, the PID controller setpoint was fixed, to test the effectiveness of the SRR device in keeping the laser output power stable. Fig. 3 summarizes the key results of these measurements. In Fig. 3 (a), the top graph shows the time variation of the laser power transmitted through the SRR modulator. The bottom graph shows the corresponding PID controller output voltage. It can be seen

that during the first 60 seconds, the PID controller is on, and the power is stabilized at around 10. At 60 seconds, the PID controller is switched off and the power starts oscillating. When the PID controller is switched on again at 153 seconds, the power returns to 10 and stabilizes. To characterize the stabilization, the QCL power was recorded in three different experimental configurations: (1) laser passing through SRR modulator with PID (2) without PID control and (3) a free running laser. Fig. 3 (b) compares the stability of the power in the three aforementioned experimental conditions, which give fluctuation magnitudes of 0.0043, 0.054, and 0.152, respectively. With the PID controlled SRR device switched on, the fluctuation of the QCL power is reduced from 1.52% to 0.043% of the total power, which is more than a 30-fold time improvement with this non-optimized stabilization approach. The PID control loop plus the modulator in the setup has a certain bandwidth, and the high frequency fluctuations of the QCL power beyond this can not be compensated, which is the main reason for the residual amplitude fluctuations.

The second experiment was designed to test the capability of active control of the QCL output power using the system. In this experiment, different waveforms were superimposed onto the PID voltage setpoint, and the corresponding laser amplitudes were recorded. Fig. 4 shows the response of the system to a 1 Hz square wave, given by a function generator. The amplitude and offset of the square waves are 0.011V and 5.188V, respectively. As can be seen, the output of the PID controller is also a square wave at the same frequency as the setpoint, but with an inverted phase. This is due to the negative feedback of the PID loop: a higher feedback signal gives lower transmittivity and thus lowers the transmission power. The QCL power followed the waveform of the setpoint with the same amplitude and frequency. There are some oscillations on the output power, which might be attributed to the variation in setpoint. This active control is effective for a time frame longer than 3 minutes, as shown in Fig. 4 (b), making it suitable for experiments in spectroscopy and communications. The time variation of the PID controller output also reveals the fluctuation of the QCL power with respect to time. We also measured the response of the system with a sine wave and a triangular wave, with the results shown in the supplementary material.

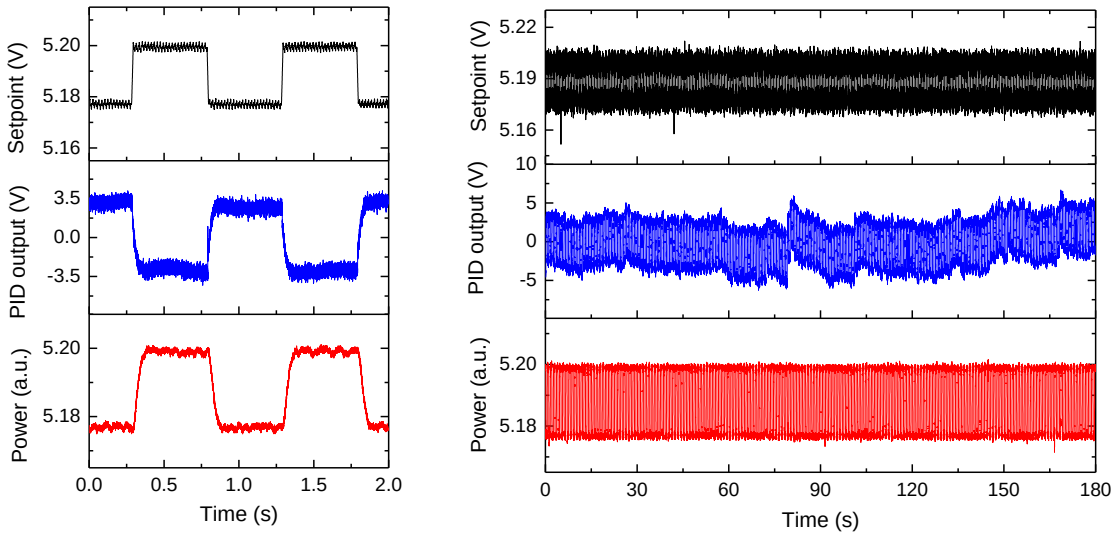

FIG. 4. The time variation of the PID controller setpoint, the PID controller output and the power of the QCL when a square wave is applied as the power setpoint: (a) in 2 seconds; (b) in 180 seconds.

In conclusion, we have demonstrated amplitude stabilization of a 2.85 THz single-plasmon QCL with a graphene loaded SRR amplitude modulator. The modulator works at room temperature and is capable of 1.6% modulation of the transmitted laser power, corresponding to a voltage setpoint at 20 V with a 20 V AC voltage superimposed. This modulation is sufficient to be used for effective laser amplitude stabilization, despite the fact that there is significant room for optimization of the demonstrated system. The magnitude of the fluctuation in laser power is reduced from 1.52% to 0.043%. The efficiency, flexibility and robustness of this approach have also been demonstrated through the use of several active control configurations for the QCL output, without affecting the amplitude stability.

See supplementary material for the current-voltage-intensity response and the spectrum of the QCL used in the setup and the response of the system to a sine wave and a triangular wave.

This work is supported by funding from the Engineering and Physical Sciences Research Council (Grant No. EP/P021859/1, HyperTerahertz–High precision terahertz spectroscopy and microscopy).

[1] D. Rabanus, U. U. Graf, M. Philipp, O. Ricken, J. Stutzki, B. Vowinkel, M. C. Wiedner, C. Walther, M. Fischer, and J. Faist, Opt. Express **17**, 1159 (2009).
[2] Y. Ren, R. Wallis, D. S. Jessop, R. Degl'Innocenti, A. Klimont, H. E. Beere, and D. A. Ritchie, Appl. Phys. Lett. **107**, 11107 (2015).
[3] R. Eichholz, H. Richter, M. Wienold, L. Schrottke, H. T. Grahn, and H. W. Hübers, Int. Conf. Infrared, Millimeter, Terahertz Waves, IRMMW-THz **21**, 32199 (2013).
[4] B. S. Williams, Nat. Photonics **1**, 517 (2007).
[5] M. S. Vitiello, L. Consolino, S. Bartalini, A. Taschin, A. Tredicucci, M. Inguscio, and P. De Natale, Nat. Photonics **6**, 525 (2012).
[6] E. F. Van Dishoeck and A. G. G. M. Tielens, in *Century Sp. Sci.* (Springer, 2001), pp. 607–645.
[7] R. Nelander and A. Wacker, Appl. Phys. Lett. **92**, 81102 (2008).
[8] Y. Ren, D. J. Hayton, J. N. Hovenier, M. Cui, J. R. Gao, T. M. Klapwijk, S. C. Shi, T.-Y. Kao, Q. Hu, and J. L. Reno, Appl. Phys. Lett. **101**, 101111 (2012).
[9] D. M. Slocum, E. J. Slingerland, R. H. Giles, and T. M. Goyette, J. Quant. Spectrosc. Radiat. Transf. **127**, 49 (2013).
[10] P. Patimisco, S. Borri, A. Sampaolo, H. E. Beere, D. A. Ritchie, M. S. Vitiello, G. Scamarcio, and V. Spagnolo, Analyst **139**, 2079 (2014).
[11] S. Koenig, D. Lopez-Diaz, J. Antes, F. Boes, R. Henneberger, A. Leuther, A. Tessmann, R. Schmogrow, D. Hillerkuss, R. Palmer, T. Zwick, C. Koos, W. Freude, O. Ambacher, J. Leuthold, and I. Kallfass, Nat. Photonics **7**, 977 (2013).
[12] I. Kallfass, J. Antes, T. Schneider, F. Kurz, D. Lopez-Diaz, S. Diebold, H. Massler, A. Leuther, and A. Tessmann, IEEE Trans. Terahertz Sci. Technol. **1**, 477 (2011).
[13] D. S. Jessop, S. J. Kindness, L. Xiao, P. Braeuninger-Weimer, H. Lin, Y. Ren, C. X. Ren, S. Hofmann, J. A. Zeitler, H. E. Beere, D. A. Ritchie, and R. Degl'Innocenti, Appl. Phys. Lett. **108**, 171101 (2016).
[14] P. Q. Liu, I. J. Luxmoore, S. A. Mikhailov, N. A. Savostianova, F. Valmorra, J. Faist, and G. R. Nash, Nat. Commun. **6**, 8969 (2015).
[15] H. Chen, W. J. Padilla, J. M. O. Zide, A. C. Gossard, A. J. Taylor, and R. D. Averitt, Nature **444**, 597 (2006).
[16] A. H. Castro Neto, F. Guinea, N. M. R. Peres, K. S. Novoselov, and A. K. Geim, Rev. Mod. Phys. **81**, 109 (2009).
[17] R. Degl'Innocenti, S. J. Kindness, H. E. Beere, and D. A. Ritchie, Nanophotonics **7**, 127 (2018).
[18] F. Valmorra, G. Scalari, C. Maissen, W. Fu, C. Schönenberger, J. W. Choi, H. G. Park, M. Beck, and J. Faist, Nano Lett. **13**, 3193 (2013).
[19] R. Degl'Innocenti, D. S. Jessop, Y. D. Shah, J. Sibik, J. A. Zeitler, P. R. Kidambi, S. Hofmann, H. E. Beere, and D. A. Ritchie, ACS Nano **8**, 2548 (2014).
[20] S. J. Kindness, D. S. Jessop, B. Wei, R. Wallis, V. S. Kamboj, L. Xiao, Y. Ren, P. Braeuninger-Weimer, A. I. Aria, S. Hofmann, H. E. Beere, D. A. Ritchie, and R. Degl'Innocenti, Sci. Rep. **7**, 7657 (2017).
[21] S. Barbieri, J. Alton, H. E. Beere, J. Fowler, E. H. Linfield, and D. A. Ritchie, Appl. Phys. Lett. **85**, 1674 (2004).
[22] R. Degl'Innocenti, L. Xiao, D. S. Jessop, S. J. Kindness, Y. Ren, H. Lin, J. A. Zeitler, J. A. Alexander-Webber, H. J. Joyce, P. Braeuninger-Weimer, S. Hofmann, H. E. Beere, and D. A. Ritchie, ACS Photonics **3**, 1747 (2016).
[23] R. Degl'Innocenti, L. Xiao, S. J. Kindness, V. S. Kamboj, B. Wei, P. Braeuninger-Weimer, K. Nakanishi, A. I. Aria, S. Hofmann, and H. E. Beere, J. Phys. D. Appl. Phys. **50**, 174001 (2017).
[24] S. Hofmann, P. Braeuninger-Weimer, and R. S. Weatherup, J. Phys. Chem. Lett. **6**, 2714 (2015).
[25] J. A. Alexander-Webber, A. A. Sagade, A. I. Aria, Z. A. Van Veldhoven, P. Braeuninger-Weimer, R. Wang, A. Cabrero-Vilatela, M.-B. Martin, J. Sui, M. R. Connolly, and S. Hofmann, 2D Mater. **4**, 11008 (2016).